Metabonomic investigations in mice infected with *Schistosoma mansoni*: An approach for biomarker identification

Yulan Wang*, Elaine Holmes*, Jeremy K. Nicholson*, Olivier Cloarec*, Jacques Chollet†, Marcel Tanner‡, Burton H. Singer§, and Jürg Utzinger‡¶

*Biological Chemistry, Biomedical Sciences Division, Faculty of Medicine, Imperial College, Sir Alexander Fleming Building, South Kensington, London SW7 2AZ, England; Departments of †Medical Parasitology and Infection Biology and ‡Public Health and Epidemiology, Swiss Tropical Institute, CH-4002 Basel, Switzerland; and §Office of Population Research, Princeton University, 245 Wallace Hall, Princeton, NJ 08544

Contributed by Burton H. Singer, July 8, 2004

Schistosomiasis, a chronic and debilitating parasitic disease, affects ≈200 million people in the developing world and imposes a substantial public health and economic impact. Accurately diagnosing at the individual level, monitoring disease progression, and assessing the impact of pharmacological interventions at the population level are of prime importance for controlling schistosomiasis. Using a *Schistosoma mansoni*–mouse model, we present a characterization of a parasitic infection by metabolic profiling, employing ^{1}H NMR spectroscopy and multivariate pattern recognition techniques. We infected 10 mice with 80 *S. mansoni* cercariae each and collected urine samples 49 and 56 days postinfection. Urine samples were also obtained from 10 uninfected control mice at the same time. The metabolic signature of an *S. mansoni* infection consists of reduced levels of the tricarboxylic acid cycle intermediates, including citrate, succinate, and 2-oxoglutarate, and increased levels of pyruvate, suggesting stimulated glycolysis. A disturbance of amino acid metabolism was also associated with an *S. mansoni* infection, as indicated by depletion of taurine, 2-oxoisocaproate, and 2-oxoisovalerate and elevation of tryptophan in the urine. A range of microbial-related metabolites, i.e., trimethylamine, phenylacetylglycine, acetate, *p*-cresol glucuronide, butyrate, propionate, and hippurate, were also coupled with an *S. mansoni* infection, indicating disturbances in the gut microbiota. Our work highlights the potential of metabolic profiling to enhance our understanding of biological responses to parasitic infections. It also holds promise as a basis for novel diagnostic tests with high sensitivity and specificity and for improved disease surveillance and control.

Schistosomiasis is a chronic and debilitating disease, which is caused by small parasitic trematode worms (schistosomes). An estimated 650 million people live at risk of infection, and 200 million people are affected, particularly the rural poor living in sub-Saharan Africa, where >85% of the current global burden is concentrated (1–3). Among the five species of schistosomes that can infect humans, *Schistosoma haematobium*, *Schistosoma japonicum*, and *Schistosoma mansoni* are of particular public health and economic significance (1–3). Heavy infections contribute to anemia and can retard children's growth, physical activity, and cognitive function. If left untreated, such infections lead to substantial morbidity, including obstructive uropathy, bladder calcification (*S. haematobium*), and periportal hepatic fibrosis (*S. japonicum* and *S. mansoni*) (2–5). Recent analyses suggest that the annual schistosome-related mortality in sub-Saharan Africa exceeds 200,000 (6).

Accurate diagnostic tests are mandatory for diagnosis at the individual level and for effective disease surveillance and control at the population level, particularly to monitor large-scale chemotherapy programs. Microscopic detection of schistosome eggs in fecal samples (*S. japonicum* and *S. mansoni*) or urine (*S. haematobium*) remains the most widely used direct diagnostic method in endemic areas (2, 3). The Kato–Katz thick smear, for example, is the most commonly used technique in epidemiological surveys that focus on *S. mansoni*. Although this method has a high specificity, is inexpensive, and requires relatively unsophisticated equipment and training, it lacks sensitivity, particularly in settings with low infection intensities (7–9). During the past 10–15 years, progress has been made with immunological methods, namely circulating antigen detection and antibody detection. Although immunoassays display some advantages over parasitological microscopy (9), wider application in both clinical and epidemiological settings remains elusive.

Enhancement of our current understanding of a host's metabolic response to a parasitic infection is a promising approach for biomarker identification, yet its potential for diagnosis and disease surveillance has been underused. Underlying reasons are that conventional biochemistry techniques for investigating changes in metabolism are time consuming and fragmentary (10, 11). Significant advances with NMR and other spectroscopy-based metabonomic techniques hold promise for overcoming these limitations. Metabonomics involves the study of multivariate metabolic response of complex multicellular organisms to pathological stressors and the consequent disruption of system regulation (12). We have shown that NMR spectroscopy, coupled with data-reduction techniques, offers a powerful approach to generate and analyze high information density metabolic data on biofluids and tissues (13). This approach is capable of simultaneously detecting a wide range of small molecule metabolites, thus providing a "metabolic fingerprint" of biofluids and tissues (12). Multivariate statistical analysis, including linear projection methods, principal component analysis (PCA), Bayesian probabilistic methods, and neural networks (14) can be applied to complex spectral data to aid visualization and characterization of changes relating to a biological perturbation. Metabonomics has become a well established analytical tool with successful applications in different fields, e.g., the study of disease processes and drug toxicity (15–18), and detection of metabolites of inborn errors (19). Recent technological advances have enabled analysis of more subtle metabolic responses to challenges such as nutritional intervention (20), variation in hormonal cycles (21), gender differences, and diurnal variation (22). Moreover, this technology has the ability to differentiate phenotypes of experimental animal models (22).

Here, we present a characterization of a parasitic infection by metabolite profiling, using a ^{1}H NMR-based analytical strategy combined with multivariate pattern recognition techniques. The experimental focus is on an *S. mansoni* infection in mouse, and the goal is to determine a metabolic signature of infection that provides the basis for accurate diagnosis and improved disease surveillance.

Abbreviations: PC, principal component; PCA, principal component analysis; PLS-DA, partial least squares-discriminant analysis; SIMCA, soft independent modeling of class analogy; TCA, tricarboxylic acid.

¶To whom correspondence should be addressed. E-mail: juerg.utzinger@unibas.ch.

www.pnas.org/cgi/doi/10.1073/pnas.0404878101

Materials and Methods

Host–Parasite Model. All experiments were carried out at the animal care facilities of the Swiss Tropical Institute by a senior laboratory technologist, adhering to standardized procedures. The study was approved by Swiss Tropical Institute's institutional review board, and the work was in compliance with Swiss national regulations. We used a *S. mansoni*–mouse model throughout this study. Twenty female mice (NMRI strain), weighing ≈20 g, were purchased from Biotechnology & Animal Breeding Division (Füllinsdorf, Switzerland). They were kept in four equally large groups and received commercial rodent food from Eberle NAFAG (Gossau, Switzerland) and water ad libitum.

Half of the mice (two groups of five mice) were infected s.c. with 80 *S. mansoni* cercariae (Liberian strain) each. Cercariae were obtained from laboratory-bred and experimentally infected *Biomphalaria glabrata* snails that served as the intermediate host after exposure to artificial light for 4 h. The *S. mansoni* life cycle has been maintained at the Swiss Tropical Institute during the past 20 years. The other 10 mice remained uninfected. Hence, they served as a control.

Urine Collection. In the early afternoon (1400) at day 49 postinfection, each infected mouse was placed in an individual metabolism cage. They were fed three aliquots of water, orally with a syringe, at hourly intervals. This approach facilitated a sufficient amount of urine being generated within a few hours so that potential time-related effects (e.g., diurnal variation) could be minimized. The metabolism cages facilitated separation of fecal material from urine, the latter collected in plastic tubes (10 ml) embedded in an ice bath at 0°C. Mice were neither fed nor given drinking water while in the metabolism cages to avoid potential contamination due to spills from diet or water in the urine collection tubes. After 3 h, between 0.7 and 1.5 ml of urine was obtained from each mouse. Urine samples were mixed thoroughly, and ≤1 ml was transferred into small plastic tubes (1.5 ml) that were firmly closed, marked with unique identification numbers, and immediately transferred into a freezer and stored at −80°C. Mice were then returned to their group cages. For the next 7 days, they were again maintained on rodent food and water.

The same procedures were repeated at day 56 postinfection for individual collection of mouse urine. The underlying rationale for selecting these two time points, i.e., urine collection 49 and 56 days after infection, was our interest in the metabolic profiling of an adult *S. mansoni* infection. Previous work had established that the development of schistosomes to reach sexual maturity and, hence, commence with egg production, takes ≥34–35 days, whereas in some worms it may take an additional 20 days (23). Finally, urine samples were also obtained from uninfected control mice at the same time points and adhering to the same procedures. In total, 40 mouse urine samples were collected. They were transferred on dry ice to Imperial College London (London) and stored at −40°C pending ^{1}H NMR spectroscopic analyses.

Dissection. Seven of the 10 *S. mansoni*-infected mice were killed by bloodletting at day 57 postinfection. They were dissected as follows. First, the liver was removed, placed into a 20 × 20 cm transparent plastic folder and gently compressed between two glass plates to obtain a flat layer of parenchyma. It was examined under a stereoscopic microscope at ×10 magnification. All live *S. mansoni* worms were sexed and counted. Second, the small and large intestines were removed and placed in a Petri dish. The mesenteric veins were examined, also under a stereoscopic microscope, at ×10 magnification. All live *S. mansoni* worms were removed, sexed, and counted.

The three remaining *S. mansoni*-infected mice were treated with a single oral dose of 400 mg/kg praziquantel Shanghai No. 6 Pharmaceutical Cooperation (Shanghai, China), the current drug of choice for the control of schistosome-attributable morbidity (1–3), for appraisal of *in vivo* effects of this drug in our experimental model. These samples were not used in metabonomic analysis.

^{1}H NMR Spectroscopy. Urine samples were prepared by mixing 400 μl of urine with 200 μl of phosphate buffer (pH 7.4), containing 10% D_2O as a field frequency lock and 0.05% sodium 3-(trimethylsilyl) propionate-2,2,3,3-d_4 as a chemical shift reference. All ^{1}H NMR spectra were recorded on a Bruker DRX 600 NMR spectrometer (Rheinstetten, Germany) operating at 600.13 MHz for ^{1}H, equipped with a flow probe. A standard 1D pulse sequence (recycle delay–90°–t_1–90°–t_m–90°–acquisition) was used. Water suppression was achieved with an irradiation on the water peak during the recycle delay (2 s) and mixing time, t_m, of 150 ms. t_1 was set to 3 μs. The 90° pulse length was adjusted to ≈10 μs. One hundred twenty-eight transients were collected into 32,000 data points for each spectrum with a spectral width of 20 ppm. All free induction decays were multiplied by an exponential function equivalent to a 0.3-Hz line-broadening factor before Fourier transformation.

For assignment purposes, 2D correlation spectroscopy (COSY) and total correlation spectroscopy (TOCSY) NMR spectra were also acquired for a urine sample. In both cases, 48 transients per increment and 256 increments were collected into 2,000 data points. The spectral width in both dimensions was 10 ppm. The TOCSY NMR spectra were acquired by using the MLEV-17 (24) spin-lock scheme for ^{1}H–^{1}H transfers with a spin-lock power of 6 kHz. The COSY spectra were recorded with gradient selection. In both 2D NMR experiments, the water signal was irradiated with a weak pulse (≈50 Hz) during the recycle delay, the data were zero-filled to 2,000 data points in the evolution dimension. Before Fourier transformation, an unshifted sine-bell and a shifted sine-bell apodization function were applied to the free induction decays from the COSY and TOCSY spectra, respectively.

Data Reduction and Pattern Recognition. ^{1}H NMR spectra were phased and baseline-corrected with an in-house developed MATLAB script (Tim Ebbels, Imperial College London, personal communication). The spectra over the range of δ 0.2–10.0 ppm were reduced by using AMIX (Bruker Analytik, Rheinstetten, Germany) to 245 regions, each 0.04 ppm wide, and the signal intensity in each region was integrated. The region δ 4.5–6.0 ppm was removed to eliminate baseline effects of imperfect water saturation. Although the urine was buffered to a close pH range, citrate is particularly susceptible to small pH changes, and for this reason citrate resonances of δ 2.72 and δ 2.68 ppm were merged to a single integral window at δ 2.70 ppm. Furthermore, citrate resonances at δ 2.56 and δ 2.52 ppm were merged to a δ 2.54 ppm integral window to take account of a pH-related peak shift.

Normalization to the total sum of the spectrum was carried out on the data before pattern recognition analyses. In the first instance, PCA was performed by using a mean-centered approach with the software SIMCA-P 10.0 (Umetrics, Umeå, Sweden). Data were visualized by using the principal component (PC) score and loading plots. Each point on the scores plot represents an individual sample, and each point on the loadings plot represents a single NMR spectral region. The score and loading plots are complementary. Thus, biochemical components responsible for the differences between samples detected in the scores plot can be extracted from the corresponding loadings. To maximize separation between the infected and noninfected samples, partial least squares-discriminant analysis (PLS-DA) was performed by using infected or noninfected as *y* variables (25). A supervised pattern recognition method, soft independent modeling of class analogy (SIMCA) (26), was also used. The data set was divided into a "training" and a "test" set, and PCs of each class in the training set were calculated. The class membership of test set samples was assigned according to their

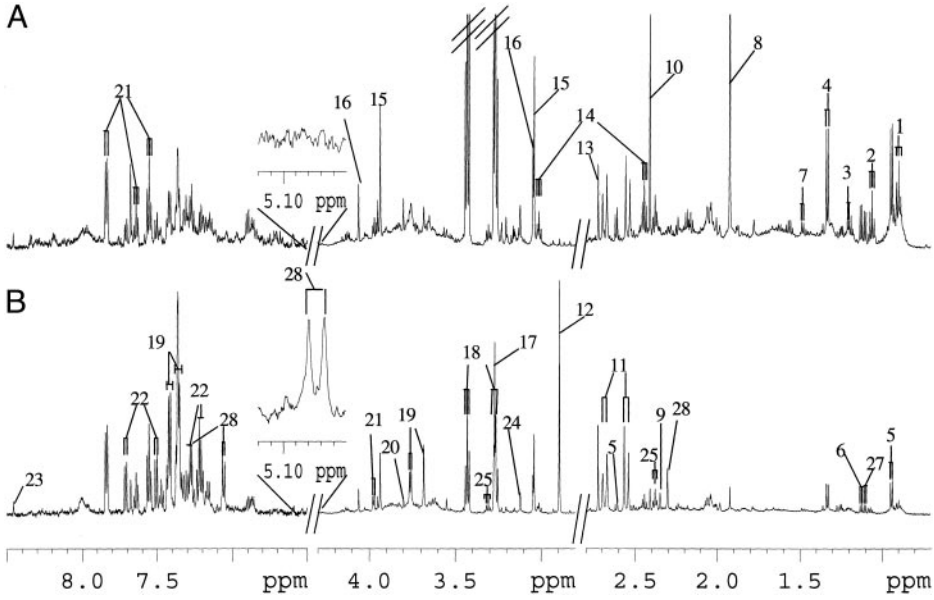

Fig. 1. Typical 600 MHz ^{1}H NMR spectra of urine obtained from an uninfected control mouse (*A*) and a mouse with a 49-day-old *S. mansoni* infection (*B*). The spectra in the aromatic region (δ 6.5–8.5) were magnified 4 times compared with the region δ 2.8–4.3, whereas the region δ 0.7–2.8 was magnified 2 times. Keys to Figs. 1 and 2: 1, butyrate; 2, propionate; 3, D-3-hydroxybutyrate; 4, lactate; 5, 2-oxoisocaproate; 6, 2-oxoisovalerate; 7, alanine; 8, acetate; 9, pyruvate; 10, succinate; 11, citrate; 12, trimethylamine; 13, dimethylamine; 14, 2-oxoglutarate; 15, creatine; 16, creatinine; 17, trimethylamine *N*-oxide; 18, taurine; 19, phenylacetylglycine; 20, guanodinoacetic acid; 21, hippurate; 22, tryptophan; 23, formate; 24, malonate; 25, β-alanine; 26, isobutyramide; 27, 2-oxoisovaleramide; 28, *p*-cresol glucuronide.

position within the calculated boundaries of the training set group, specified in a Cooman's residual plot (27).

To aid the identification of metabolites that differed significantly between the *S. mansoni*-infected and uninfected mice, additional analyses were performed. We used a combination of optimized scaling and examination of the sample–sample correlation matrix to aid direct ranking of resonances correlated to selected signals of interest employing this method (28).

Results

***S. mansoni* Infection.** At day 57 postinfection, 19–40 live *S. mansoni* worms were recovered (mean: 29.7; SD: 7.9), primarily from the mesenteric veins, from the seven mice killed at this time point. This indicates that one-quarter to one-half of *S. mansoni* cercariae developed into adult worms, which is in agreement with our preceding work in the same host–parasite model (29) and recent findings presented by others (30).

^{1}H NMR Spectroscopy of Mouse Urine. An example of ^{1}H NMR spectra of a urine sample obtained from an uninfected control mouse (*A*) and a mouse with a 49-day-old *S. mansoni* infection (*B*) is shown in Fig. 1. Resonance assignments were made according to the literature (31) and confirmed by 2D COSY (Fig. 2) and total correlation spectroscopy. The spectra were dominated by a number of metabolites, including acetate, alanine, β-alanine, 2-oxoglutarate, 2-oxoisocaproate, 2-oxoisovalerate, butyrate, D-3-hydroxybutyrate, citrate, creatine, creatinine, *p*-cresol glucuronide, formate, dimethylamine, hippurate, isovalerate, lactate, malonate, phenylacetylglycine, propionate, pyruvate, succinate, taurine, trimethylamine, trimethylamine *N*-oxide, and tryptophan, which could all be directly assigned. Visual inspection of the spectra revealed differences in overall composition between urines obtained from control animals and *S. mansoni*-infected mice. For example, elevated levels of lactate and trimethylamine, but depletion of alanine, 2-oxoisocaproate, 2-oxoisovalerate, butyrate, D-3-hydroxybutyrate, citrate, isovalerate, propionate, and taurine were observed in urine of *S. mansoni*-infected mice. However, visual analysis of the ^{1}H NMR spectral profiles of the urine samples is a subjective process, and interanimal variation can distort interpretation of the data. PCA was performed to facilitate a general overview of metabolite patterns and to identify biomarkers that may give rise to diagnosis of an *S. mansoni* infection.

PCA of ^{1}H NMR Data. PCA was carried out on the normalized NMR dataset by using mean-centered data. The PCA scores plot from urines of uninfected control and *S. mansoni*-infected mice, collected at day 49 postinfection (and at the same time for uninfected control mice) is shown in Fig. 3*A*. The urine samples recovered 7 days later (i.e., 56 days postinfection) showed a similar separation between infected and uninfected mice. Four components were calculated and the model corresponding to the first four PCs explained 84% of the total variance. Separation between the *S. mansoni*-infected and the uninfected control mice was achieved predominately in the third PC (Fig. 3*A*). Having demonstrated clustering related to infection status by using PCA, we subsequently investigated the data by using PLS-DA to maximize the separation between infected and control animals (Fig. 3*B*). A clear separation between the classes was found in the first component. The dominant metabolites influencing the differentiation between control and infected mice are listed in Table 1 together with a measure of their relative influence on the model given by the variable importance parameter. The largest

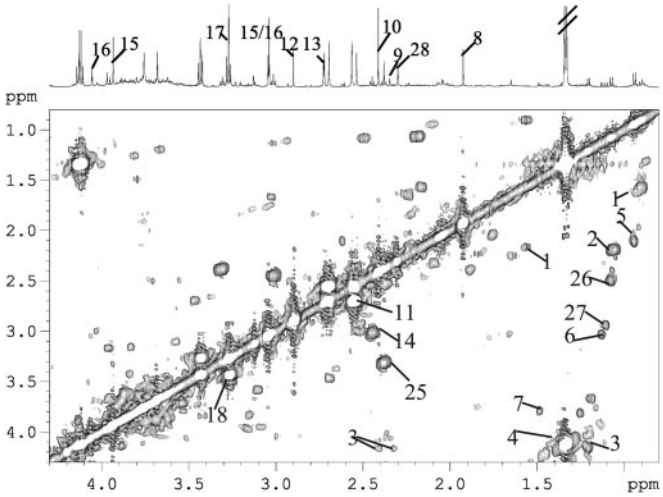

Fig. 2. COSY spectrum of an *S. mansoni*-infected mouse urine acquired at 600 MHz in an ^{1}H NMR spectrometer. The cross peaks indicate adjacent protons. For keys, see Fig. 1 legend.

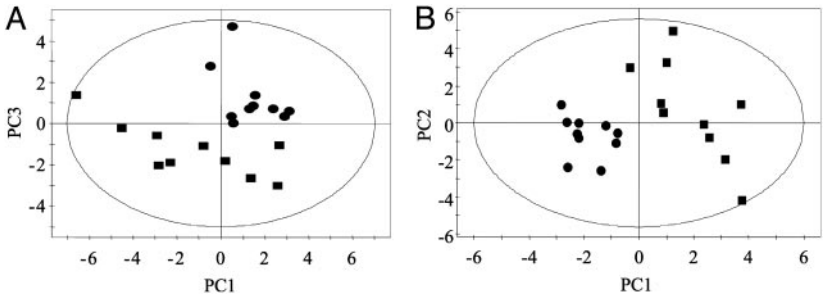

Fig. 3. PCA (*A*) and PLS-DA (*B*) scores plots derived from PCA of ^{1}H NMR spectra of urines collected from mice with 49-day-old *S. mansoni* infections (■) or from uninfected control mice (●).

influence on the separation between *S. mansoni*-infected and uninfected mice was increased urinary excretion of trimethylamine and phenylacetylglycine, as well as decreased urinary excretion of citrate, acetate, and taurine (Table 1).

When mean-centered data without an *a priori* requirement of scaling are used, the results lead to an overestimation of those metabolites that are present at high concentrations with corresponding high variances. Thus, to extract potentially influential metabolites that are present only at relatively low concentrations, further modification of our analytical approach was initiated. Biomarkers at high concentrations that discriminated between infected and uninfected mice, namely trimethylamine (δ 2.88), phenylacetylglycine (δ 7.36, δ 3.76, δ 3.68), citrate (δ 2.54, δ 2.70), acetate (δ 1.92), and taurine (δ 3.24, δ 3.28, δ 3.40, δ 3.44), were removed from the initial dataset. Lactate (δ 1.32, δ 4.12) concentration varied between animals but was not found to be significant in discriminating between *S. mansoni*-infected and control mice. To eliminate this effect, lactate resonance was also removed. Subsequent PCA and PLS-DA were performed on the renormalized dataset after the removal of the NMR regions corresponding to the above-mentioned chemical shifts. After reanalysis of this modified dataset, one sample from the *S. mansoni*-infected group (day 49) was excluded, because it clustered with the control samples and showed no metabolic response to the infection. Now, the *S. mansoni*-infected and the uninfected control samples were clearly differentiated in the PC1 (Fig. 4). The metabolites exerting the strongest leverage on the separation between the two groups were elevated levels of creatine, tryptophan, and pyruvate, and depleted levels of hippurate, a range of short-chain fatty acids including butyrate and propionate, and β-alanine (δ 2.32, δ 3.32). In addition, 2-oxoisocaproate, 2-oxoisovalerate, D-3-hydroxybutyrate, alanine, malonate, and tricarboxylic acid (TCA) cycle intermediates 2-oxoglutarate and succinate showed lower levels in the urines obtained from *S. mansoni*-infected mice (Table 1). Use of optimized scaling and sample–sample correlation analysis resulted in the clear identification of *p*-cresol glucuronide in the urine of mice infected with *S. mansoni*. This metabolite was not present in observable quantities in the urine from uninfected animals.

Table 1. The changes of metabolites observed in urines obtained from *S. mansoni*-infected mice compared with uninfected control mice and the importance of contributions

Metabolite (key*)	Chemical shift δ, ppm	Changes direction	Importance of contribution (rank)
Trimethylamine (12)	2.88	↑	7.547† (1)
Phenylacetylglycine (19)	7.36, 3.76, 3.68	↑	3.196†, 2.957†, 2.767† (2)
Taurine (18)	3.24, 3.28, 3.40, 3.44	↓	1.664†, 1.608†, 1.159†, 6.504† (3)
Citrate (11)	2.54, 2.70	↓	3.553†, 2.782† (4)
Acetate (8)	1.92	↓	2.663† (5)
Creatine (15)	3.04, 3.92	↑	5.671, 4.234 (1)
β-Alanine (25)	2.32, 3.32	↑	3.308, 1.934 (2)
Pyruvate (9)	2.36	↑	2.946 (3)
2-Oxoisocaproate (5)	0.92, 2.64	↓	2.746, 1.064 (4)
Tryptophan (22)	7.24, 7.28, 7.52, 7.71	↑	2.391, 1.945, 0.914, 0.999 (5)
Hippurate (21)	7.84, 7.64, 7.56, 3.96	↓	2.137, 1.005, 0.415, 0.997 (6)
Butyrate (1)	0.88, 1.56	↓	1.487, 1.484 (7)
p-Cresol glucuronide (28)	3.88, 3.84, 7.08, 7.04,	↑	1.487, 1.438, 1.303, 1.217 (8)
Succinate (10)	2.44	↓	1.350 (9)
Malonate (24)	3.16	↓	1.204 (10)
Propionate (2)	1.04, 2.16	↓	1.093, 1.717 (11)
2-Oxoglutarate (14)	2.46, 3.00	↓	0.890, 0.704 (12)
Alanine (7)	1.48	↓	0.889 (13)
2-Oxoisovalerate (6)	1.12	↓	0.619 (14)
D-3-Hydroxybutyrate (3)	1.20	↓	0.554 (15)

The arrows indicate the direction of the change (↑, increase; ↓, decrease) in the concentration among *S. mansoni*-infected mice relative to the uninfected control animals.

*Key numbers correspond with metabolite's place on 600-MHz NMR spectra in Fig. 1.

†Variable importance parameters were generated from model 1 corresponding to Fig. 3, and the remaining were generated from the model 2 corresponding to Fig. 4.

SIMCA Analysis of the ^{1}H NMR Data. Because good separation between the uninfected control and the *S. mansoni*-infected mice was observed by PCA without any *a priori* assumptions regarding classification of the sample, the data were further analyzed by using SIMCA. This method applies knowledge of class membership, i.e., control or infected, to maximize the separation between the classes. As with other supervised techniques, it is essential to test the model with an independent test set to establish the robustness of the model, thereby defining the level of predictability. To assess whether predictions of *S. mansoni* infections from mouse urine samples are possible, PCA models were established by using half of the infected and half of the controls separately, each with the first three PCs. A SIMCA

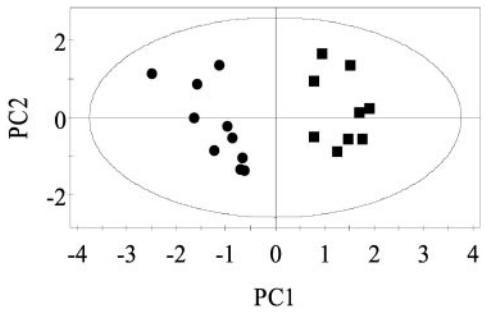

Fig. 4. PC1 vs. PC2 scores plot from ^{1}H NMR spectra of urine from *S. mansoni*-infected (■) and uninfected control (●) mice after resonance from trimethylamine (δ 2.88), phenylacetylglycine (δ 7.36, δ 3.76, δ 3.68), citrate (δ 2.54, δ 2.70), acetate (δ 1.92), lactate (δ 1.32, δ 4.12), and taurine (δ 3.24, δ 3.28, δ 3.40, δ 3.44) was removed.

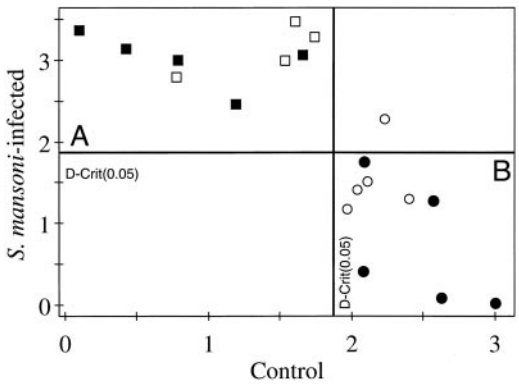

Fig. 5. Cooman plot of 600-MHz ^{1}H NMR spectra of urine from *S. mansoni*-infected mice from the training set (■), uninfected control mice from the training set (●), infected mice from the test set (□), and control mice from the test set (○).

model was then constructed with a view toward establishing the class membership for the remaining half of the dataset. Fig. 5 shows the Cooman residual plot of membership of uninfected control and *S. mansoni*-infected mice. The plot was divided into four regions by 95% confidence limit lines for both classes. The test set distributed in region A (upper left) was classified as the infected group, whereas the control group was in region B (lower right). The entire test set from the infected group (□) and four of the five from the controls (○) were correctly predicted and cross validated. The remaining control sample was not predicted as belonging to any class but as an "unknown." Visual examination of this sample showed that the urinary profile contained relatively more creatine than did other control samples from the uninfected control group.

Discussion

This application of metabonomics for class discrimination and biomarker identification in parasitic infections clarifies the potential of this methodology for accurate disease diagnosis and as a tool for improved disease surveillance. The feasibility of the metabonomic approach in assessing chronic disease conditions has been demonstrated recently. NMR spectra of human serum, accompanied by appropriate pattern recognition techniques, provided a rapid, accurate, and noninvasive methodology for diagnosis of coronary heart disease and the assessment of its severity (32).

In the present study, the focus was on an experimental infection of *S. mansoni* in a mouse model. NMR spectra were derived from urine samples, collected, and analyzed under standardized procedures. No attempt was made for metabonomic analyses of blood plasma because an important aim of our work is to develop an accurate and noninvasive diagnostic test for *S. mansoni* infections in humans. Today's gold standard for diagnosis in epidemiological surveys in endemic areas is by means of stool collection and the Kato–Katz thick smear, which detects parasite eggs by microscopy (7–9). Clearly blood collection would be more invasive and, hence, compromise patients' compliance. On the other hand, collection of urine instead of stool samples is more straightforward and less invasive. A prominent finding was the depletion of the TCA cycle intermediates, including citrate, succinate, and 2-oxoglutarate, in urine samples from *S. mansoni*-infected mice, when compared with samples obtained from uninfected animals. Our results are consistent with a study performed in the same host–parasite model, where a marked reduction of citrate synthase in *S. mansoni*-infected mice was reported in ref. 33, but employing conventional biochemical analytical methods. Our findings also indicate that an infection with *S. mansoni* inhibits pyruvate dehydrogenase, which in turn explains the observed increase in pyruvate and the insufficient level of acetyl-CoA (Ac-CoA) formation for TCA cycle metabolism. In the study mentioned above, a notable increase of enzyme activities involved in carbohydrate metabolism, i.e., pyruvate kinase and phosphofructokinase, was also observed in *S. mansoni*-infected mice, commencing 4 weeks postinfection (33). These increased activities will accelerate conversion of glucose to pyruvate, which may also contribute to the elevation of pyruvate observed in the current study.

The most important clinical complication of a chronic *S. mansoni* infection in humans is periportal hepatic fibrosis, which is the result of the accumulation of collagen in the liver (3). In the current study, we observed impaired liver function in the urinary metabolites of mice already at day 49 postinfection. Depleted levels of 2-oxoisovalerate and 2-oxoisocaproate, which originate from valine and leucine, respectively, were observed in the *S. mansoni*-infected mice. This result suggests a perturbation of amino acids metabolism. This finding is consistent with the observation of an elevated level of leucine in serum of schistosome-infected patients from Egypt (34). The reduction of the D-3-hydroxybutyrate is another indication of impaired liver function because D-3-hydroxybutyrate is produced primarily by liver during oxidation of fatty acids. Alternatively, the observed depletion in D-3-hydroxybutyrate levels and in key TCA cycle intermediates may imply an alteration in the utilization of renal carbohydrate sources by the mitochondria. Hence, further studies to investigate mitochondrial metabolism in both the liver and kidney of *S. mansoni*-infected mice are needed. Although the liver carries the main burden of *S. mansoni* infection, increased prevalence of glomerulonephronephrosis can also be associated with infection (35).

In patients with intestinal schistosomiasis, splenomegaly is the usual accompaniment because of portal venous hypertension and other causes. Kidney pathology can also occur in *S. mansoni* infections and can even lead to renal failure, particularly among late-stage hepatosplenic cases (3). A possible underlying metabolic pathway of renal failure is a depressed level of TCA cycle intermediates. Urinary output of citrate is severely reduced, and this will directly impact on calcium complexation (11). Hence, reduction of urinary citrate may lead to precipitation of calcium salts in the kidney, causing malfunction. This finding has been reported in patients treated with acetazolamide for glaucoma, and this is a side effect of renal carbonic anhydrase inhibition, which reduces urinary citrate levels markedly (36).

Disturbance of amino acid metabolism may also explain the observed depletion of urinary taurine, which is derived from cysteine (37). Furthermore, the elevation of tryptophan noted in the current study is consistent with a previous study, documenting impaired tryptophan metabolism associated with *S. mansoni* infections in humans and mice (38). The reduction in alanine excretion observed in the *S. mansoni*-infected mice may imply that conversion of pyruvate to alanine by alanine aminotransferase is depressed. This result is in agreement with elevated pyruvate observed in *S. mansoni*-infected mice.

In addition to disturbance of carbohydrate metabolism and the TCA cycle and impaired liver function associated with an *S. mansoni* infection, we observed elevated levels of trimethylamine, phenylacetylglycine, and *p*-cresol glucuronide simultaneously in the ^{1}H NMR spectra of urine obtained from *S. mansoni*-infected mice. Trimethylamine is derived from intestinal degradation of food components such as choline and carnitine by the microbiota (39, 40). Previous research reported increased phenylacetylglycine in rat urine in the case of drug-induced phospholipidsosis (41) and triggered by microbial infection (42). Because diet was kept the same for the uninfected control and the *S. mansoni*-infected mice in the current study, the elevated excretion of urinary trimethylamine, phenylacetylglycine, and *p*-cresol glucuronide found in the infected animals may have been due to an increased supply from microbial agents caused by disturbance of the normal microbial ecosystem in the presence of *S. mansoni* worms. Alternatively, the

reduction of hippurate excretion and increase of *p*-cresol glucuronide may suggest an alteration in phase I and phase II metabolism. Increased activity of cytochrome P450 in the livers of *S. mansoni*-infected mice has been demonstrated in ref. 43 and may impact on subsequent phase II metabolism such as glycine and glucuronide conjugation. From these observed changes in urinary metabolite signature, it would appear that a three-way interaction may occur between the host, the parasite, and the resident host microflora.

A reduction in the concentration of short-chain fatty acids such as acetate, butyrate, and propionate was characteristic of urine samples obtained from *S. mansoni*-infected mice. These short-chain fatty acids are produced by bacteria in the colon through fermentation of unabsorbed dietary fiber and provide an energy source for metabolism in the colon. The presence of adult *S. mansoni* worms could contribute to the depletion of the short-chain fatty acids by inhibiting either the manufacture of products or the utilization of these products. The reduced excretion of urinary hippurate may also be associated with the disturbance of microbial colonies. In fact, variations of urinary hippurate concentration have been linked to changes in the distribution of intestinal microbial colonies (42, 44). Mammalian metabolism is known to be significantly influenced by interaction with its complex gut microbial community (45, 46). Recent studies have indicated that particular species of microbiota are at least partially responsible for observable differences in toxicity or susceptibility to disease. For example, certain strains of gut *Escherichia coli* have been shown to metabolize environmental toxins such as dimethylarsine into potentially highly toxic micrometabolites that relate to the gut carcinogenicity of the compound (47). The introduction of parasites into the mammalian system may displace the baseline mammalian-to-microbial behavior, thereby causing a disruption in microbial populations and, hence, in metabolism. *In vitro* studies have shown that *S. mansoni* eggs take up thymidine, uridine, and amino acids and incorporate them into DNA, RNA, and proteins (48). In our view, research is warranted to enhance our understanding of metabolic effects of *S. mansoni* on microbes and to further elucidate the host–parasite–microflora "transgenomic" metabolic cross talk. Until such results are available, conclusions with respect to disturbances of microbial colonization must be regarded as tentative. Host–parasite interactions have been shown to affect the prevalence and/or severity of pathology. For example, *S. mansoni* infection is inversely associated with response to aeroallergens (49). Deeper comprehension of the effects of an *S. mansoni* infection on the vertebrate host may also give insight into altered susceptibility to other parasitic infections or nutritional states.

In conclusion, consistent differences in the urinary metabolite profiles of mice infected with adult *S. mansoni* worms and age- and sex-matched uninfected control animals were identified with an NMR-based metabonomic strategy. Furthermore, a SIMCA model based on the ^{1}H NMR-spectral profiles allowed characterization and prediction of infected and uninfected mice. These findings highlight the potential of metabonomics as a novel approach for fundamental investigations of host–pathogen interactions as well as for disease surveillance and control. It holds promise for development of novel diagnostic approaches at individual and population levels. Future studies should look at extending this work to other host–parasite models, e.g., hamsters infected with *S. japonicum*, and investigating human subjects infected with other trematodes (e.g., *Fasciola hepatica*), nematodes (e.g., hookworm infections), and intestinal protozoa (e.g., *Entamoeba histolytica*). An innovative proteonomics approach has just been developed as an accurate diagnostic test for human African trypanosomiasis, by means of mass spectrometry on serum coupled with the use of sophisticated data mining tools (50). We believe that metabonomics also represents an "omics" science that now requires comprehensive assessment and validation for its potential in individual and community diagnosis, particularly with regard to responses to treatment. Metabonomics, in itself, represents a full systems biological approach for identifying genetic, environmental, and host–parasite metabolic interaction in whole organisms (12).

We thank Dr. T. Ebbels for allowing us to use NMRPROG to process NMR data. This work received financial support from the Roche Research Foundation, Swiss National Science Foundation Project PPOOB-102883 (to J.U.), Nestle (to Y.W.), and the Wellcome Trust (to O.C.).

1. Utzinger, J. & Keiser, J. (2004) *Expert Opin. Pharmacother.* **5,** 263–285.
2. World Health Organization (2002) *WHO Tech. Rep. Ser.* **912,** 1–57.
3. Davis, A. (2003) in *Manson's Tropical Diseases*, eds. Cook, G. & Zumla A. I. (Saunders, Philadelphia), pp. 1431–1469.
4. Hatz, C. F. R. (2001) *Adv. Parasitol.* **48,** 225–284.
5. Richter, J. (2003) *Acta Trop.* **86,** 161–183.
6. van der Werf, M. J., de Vlas, S. J., Brooker, S., Looman, C. W. N., Nagelkerke, N. J. D., Habbema, J. D. F. & Engels, D. (2003) *Acta Trop.* **86,** 125–139.
7. de Vlas, S. J. & Gryseels, B. (1992) *Parasitol. Today* **8,** 274–277.
8. Utzinger, J., Booth, M., N'Goran, E. K., Müller, I., Tanner, M. & Lengeler, C. (2001) *Parasitology* **122,** 537–544.
9. Doenhoff, M. J., Chiodini, P. L. & Hamilton, J. V. (2004) *Trends Parasitol.* **20,** 35–39.
10. Gartland, K. P. R., Beddell, C. R., Lindon, J. C. & Nicholson, J. K. (1991) *Mol. Pharmacol.* **39,** 629–642.
11. Nicholson, J. K., Timbrell, J. A. & Sadler, P. J. (1985) *Mol. Pharmacol.* **27,** 644–651.
12. Nicholson, J. K. & Wilson, I. D. (2003) *Nat. Rev. Drug Discov.* **2,** 668–676.
13. Nicholson, J. K., Lindon, J. C. & Holmes, E. (1999) *Xenobiotica* **29,** 1181–1189.
14. Holmes, E., Nicholson, J. K. & Tranter, G. (2001) *Chem. Res. Toxicol.* **14,** 182–191.
15. Robosky, L. C., Robertson, D. G., Baker, J. D., Rane, S. & Reily, M. D. (2002) *Comb. Chem. High Throughput Screen.* **5,** 651–662.
16. Holmes, E., Nicholson, J. K., Nicholls, A. W., Lindon, J. C., Connor, S. C., Polley, S. & Connelly, J. (1998) *Chemometrics Intell. Lab. Syst.* **44,** 245–255.
17. Gavaghan, C. L., Holmes, E., Lenz, E., Wilson, I. D. & Nicholson, J. K. (2000) *FEBS Lett.* **484,** 169–174.
18. Damyanovich, A. Z., Staples, J. R., Chan, A. D. M. & Marshall, K. W. (1999) *J. Orthopaed. Res.* **17,** 223–231.
19. Moolenaar, S. H., Engelke, U. F. H. & Wevers, R. A. (2003) *Ann. Clin. Biochem.* **40,** 16–24.
20. Solanky, K. S., Bailey, N. J. C., Beckwith-Hall, B. M., Davis, A., Bingham, S., Holmes, E., Nicholson, J. K. & Cassidy, A. (2003) *Anal. Biochem.* **323,** 197–204.
21. Bollard, M. E., Holmes, E., Lindon, J. C., Mitchell, S. C., Branstetter, D., Zhang, W. & Nicholson, J. K. (2001) *Anal. Biochem.* **295,** 194–202.
22. Gavaghan, C. L., Wilson, I. D. & Nicholson, J. K. (2002) *FEBS Lett.* **530,** 191–196.
23. Clegg, J. A. (1965) *Exp. Parasitol.* **16,** 133–147.
24. Bax, A. & Davis, D. G. (1985) *J. Magn. Reson.* **65,** 355–360.
25. Eriksson, L., Johansson, E., Kettanah-Wold, N. & Wold, S. (1999) *Introduction to Multi and Megavariate Data Analysis Using Project Methods (PCA and PLS-DA)* (Umetrics, Malmo, Sweden).
26. Wold, S. (1976) *Pattern Recognition* **8,** 127–139.
27. Holmes, E., Nicholls, A. W., Lindon, J. C., Ramos, S., Spraul, M., Neidig, P., Connor, S. C., Connelly, J., Damment, S. J. P., Haselden, J., *et al.* (1998) *NMR Biomed.* **11,** 235–244.
28. Cloarec, O., Dumas, M., Craig, A., Barton, R. H., Blancher, C., Gauguier, D., Lindon, J. C., Holmes, E. & Nicholson, J. K. (2004) *Anal. Chem.*, in press.
29. Utzinger, J., Chollet, J., Tu, Z. W., Xiao, S. H. & Tanner, M. (2002) *Trans. R. Soc. Trop. Med. Hyg.* **96,** 318–323.
30. Pica-Mattoccia, L. & Cioli, D. (2004) *Int. J. Parasitol.* **34,** 527–533.
31. Nicholson, J. K., Foxall, P. J. D., Spraul, M., Farrant, R. D. & Lindon, J. C. (1995) *Anal. Chem.* **67,** 793–811.
32. Brindle, J. T., Antti, H., Holmes, E., Tranter, G., Nicholson, J. K., Bethell, H. W. L., Clarke, S., Schofield, P. M., McKilligin, E., Mosedale, D. E., *et al.* (2002) *Nat. Med.* **8,** 1439–1444.
33. Ahmed, S. A. & Gad, M. Z. (1995) *Arzneim.-Forsch.* **45,** 1324–1328.
34. Ahmed, S. A. & Gad, M. Z. (1996) *Dis. Markers* **13,** 19–29.
35. Lambertucci, J. R., Serufo, J. C., Gerspacher-Lara, R., Rayes, A. A. M., Teixeira, R., Nobre, V. & Antunes, C. M. F. (2000) *Acta Trop.* **77,** 101–109.
36. Higashihara, E., Nutahara, K., Takeuchi, T., Shoji, N., Araie, M. & Aso, Y. (1991) *J. Urol.* **145,** 942–948.
37. Devlin, T. M. (1997) in *The Textbook of Biochemistry with Clinical Correlations*, ed. Devlin, T. M. (Wiley–Liss, New York), 4th Ed., p. 473.
38. Njagi, E. N. M., Bender, D. A. & Okelo, G. B. A. (1992) *Parasitology* **104,** 433–441.
39. Smith, J. L., Wishnok, J. S. & Deen, W. M. (1994) *Toxicol. Appl. Pharmacol.* **125,** 296–308.
40. Seibel, B. A. & Walsh, P. J. (2002) *J. Exp. Biol.* **205,** 297–306.
41. Nicholls, A. W., Nicholson, J. K., Haselden, J. N. & Waterfield, C. J. (2000) *Biomarkers* **5,** 410–423.
42. Nicholls, A. W., Mortishire-Smith, R. J. & Nicholson, J. K. (2003) *Chem. Res. Toxicol.* **16,** 1395–1404.
43. Sheweita, S. A., Mangoura, S. A. & El Shemi, A. G. (1998) *J. Helminthol.* **72,** 71–77.
44. Goodwin, B. L., Ruthven, C. R. J. & Sandler, M. (1994) *Biochem. Pharmacol.* **47,** 2294–2297.
45. Gordon, J. I., Stappenbeck, T. S. & Hooper, L. V. (2003) *Trends Microbiol.* **11,** 150–151.
46. Xu, J., Bjursell, M. K., Himrod, J., Deng, S., Carmichael, L. K., Chiang, H. C., Hooper, L. V. & Gordon, J. I. (2003) *Science* **299,** 2074–2076.
47. Yoshida, K., Kuroda, K., Zhou, X., Inoue, Y., Date, Y., Wanibuchi, H., Fukushima, S. & Endo, G. (2003) *Chem. Res. Toxicol.* **16,** 1124–1129.
48. Stjernholm, R. L. (1974) *Exp. Parasitol.* **36,** 222–232.
49. Araujo, M. I., Lopes, A. A., Medeiros, M., Cruz, A. A., Sousa-Atta, L., Sole, D. & Carvalho, E. M. (2000) *Int. Arch. Allergy Immunol.* **123,** 145–148.
50. Papadopoulos, M. C., Abel, P. M., Agranoff, D., Stich, A., Tarelli, E., Bell, B. A., Planche, T., Loosemore, A., Saadoun, S., Wilkins, P., *et al.* (2004) *Lancet* **363,** 1358–1363.